Journal of Catalysis **184,** 202–212 (1999)
Article ID jcat.1999.2439, available online at http://www.idealibrary.com on IDEAL®

A Transient Kinetic Study of the Carbon Dioxide Reforming of Methane over Supported Ru Catalysts

P. Ferreira-Aparicio,* C. Márquez-Alvarez,† I. Rodríguez-Ramos,* Y. Schuurman,† A. Guerrero-Ruiz,‡,[1] and C. Mirodatos†,[1]

*Instituto de Catálisis y Petroleoquímica, CSIC, Campus Cantoblanco 28049, Madrid, Spain; †Institut de Recherches sur la Catalyse, CNRS, 2 Avenue Albert Einstein, 69626, Villeurbanne Cedex, France; and ‡Departamento Química Inorgánica y Técnica. Facultad de Ciencias, UNED 28040 Madrid, Spain

Received October 14, 1998; revised January 19, 1999; accepted January 25, 1999

Carbon dioxide reforming of methane has been studied over ruthenium catalysts supported on silica, γ-alumina, and a high surface area graphite. Transient kinetic analysis and temporal analysis of products were used to unravel the reaction mechanism and point out the specificity of each support.

Over silica support, the most inert material, the whole reforming process occurs on the ruthenium phase and the fast ageing of the catalyst is related to a large residence time of surface carbon intermediates favouring polymerisation and graphitisation. Over graphite the support acts as a collector of CH_x species which reduces the residence time of carbon species on the Ru phase and therefore leads to a very stable catalyst. Over alumina support the dry reforming of methane involves a complex reaction network in which the alumina hydroxyl groups feed continuously the active Ru phase in H and O adspecies, which also limits the catalyst ageing. Accumulation of CO_x adspecies on alumina also occurs during the reaction.

Key Words: **carbon dioxide reforming of methane; transient kinetic studies; mechanism; ruthenium; effect of support.**

1. INTRODUCTION

The production of syngas by means of the carbon dioxide reforming of methane is a promising route which may compete with the classical steam reforming due to: (i) a more favourable H_2/CO ratio for Fischer–Tropsch and methanol synthesis (1–4), (ii) a higher endothermicity ($\Delta H = 260$ vs 226 kJ/mol) that allows a better utilisation in chemical energy transmission systems (CETS) (5), and (iii) the fact that both methane and carbon dioxide are known to be harmful gases responsible for the greenhouse effect.

Most of the group VIII elements are known to be active for the dry reforming. Among them, noble metals and, in particular, ruthenium and rhodium have been shown to be the most active catalysts in addition to limited carbon deposition (6, 7). Over Ru on alumina, Mark and Maier (8) propose a mechanism where the dissociative methane adsorption is rate limiting, followed by the direct reaction of CO_2 with adsorbed carbon. They observed no effect of the support on the reaction rate. Erdöhelyi *et al.* (9) observed as well no effect of the support (TiO_2, Al_2O_3, MgO, SiO_2) over Rh, but they did observe an effect over Pd. In contrast, we recently found an active role of the support in the reaction mechanism by comparing silica and alumina supported catalysts, respectively Ni/SiO_2 to Ni/Al_2O_3 and Ru/SiO_2 to Ru/Al_2O_3 (10, 11). Bitter *et al.* (12) also found that the catalytic activity of Pt/ZrO_2 is determined by the available Pt–ZrO_2 interface, while for Rh, the support plays a minimal role.

In order to investigate thoroughly this apparent sensitivity of the dry reforming to the nature of the support, transient kinetic techniques have been used to study three ruthenium catalysts dispersed on different carriers: γ-alumina, silica, and a high surface area graphite (HSAG). Steady-state isotopic transient kinetics analysis (SSITKA) and temporal analysis of products (TAP) have been proved to be powerful and sensitive techniques to unravel reaction pathways and to apply perfectly to the various reactions dealing with methane activation (10, 11, 13–16).

2. EXPERIMENTAL

2.1. Catalysts

Three different supports have been used to prepare ruthenium catalysts: γ-alumina (Puralox Condea; BET surface area = 175 m^2/g), silica (Aerosil 200, Degussa; BET surface area = 180 m^2/g), and a commercial high surface area graphite (Lonza Ltd.; BET surface area = 300 m^2/g). Impregnation of the alumina and silica supports was carried out with aqueous solutions of ruthenium chloride supplied by Aldrich Chemie. After impregnation, the catalysts were dried overnight at room temperature. In order to decompose the precursor salt, the samples were also calcined in air at 773 K for 3 h. The graphite-supported catalyst was

[1] To whom correspondence should be addressed.

0021-9517/99 $30.00

prepared by impregnation with hexane solution of high purity $Ru_3(CO)_{12}$ (Panreac). The sample was heated in air at 373 K for 8 h to remove the solvent and subsequently the precursor was decomposed in He flow at 473 K for 30 min.

Metal content in each catalyst was determined by atomic absorption. A metal loading of approximately 1 wt% was achieved for each support. Metal dispersion was measured by H_2 pulse chemisorption at 373 K for the oxide-supported catalysts and by CO chemisorption at room temperature in a volumetric system for Ru/HSAG (it was checked on similar material that the metal dispersion was very little dependent on the nature of the probe molecule, CO or H_2). Before testing, the catalysts were reduced *in situ* in pure hydrogen (20 ml min^{-1}) at 673 K for 2 h.

2.2. Steady-State Catalytic Experiments

The catalytic activity was evaluated at 823 K in a flow reaction system working at atmospheric pressure. Then, 25 to 50 mg of catalyst placed between two quartz wool plugs were loaded into a 4-mm ID tubular quartz reactor. A mixture of CH_4, CO_2, and He in a 10 : 10 : 80 volume ratio, respectively, was fed at a total flow rate of 100 ml min^{-1}.

The concentration of CH_4, CO_2, CO, and H_2 in the gas phase was determined by gas chromatography, using a TCD detector. Apart from these gases, only water was detected, though not quantified. Due to the high conversion levels, the reaction rates referred to are volume-averaged reaction rates.

2.3. Transient Kinetic Experiments

Transient kinetic experiments were carried out in an atmospheric pressure flow system using a tubular quartz micro-reactor (4-mm ID). The transient changes in gas feed composition were performed on switching a four-way valve placed just at the inlet of the reactor. The gas composition at the reactor outlet was continuously monitored by on-line mass spectrometry (MS); it was also analysed periodically by gas chromatography (TCD and FID detectors) (17).

A series of four non-steady-state transient experiments were carried out at 823 K for each catalyst. The sequence of each transient is reported in Table 1.

SSITKA experiments were performed by switching from a reaction mixture $^{12}CH_4/^{12}CO_2/He = 10 : 10 : 80$ (total flow rate of 50 ml min^{-1}), to the equivalent mixture containing $^{13}CH_4$ instead of $^{12}CH_4$ and traced with argon.

For all transient experiments, gas phase composition was calculated from the MS signal at the following m/e ratios: 40 (Ar), 15 ($^{12}CH_4$), 17 ($^{13}CH_4$), 44 ($^{12}CO_2$), 45 ($^{13}CO_2$), 28 (^{12}CO), 29 (^{13}CO), 2 (H_2), and 18 (H_2O). The fragmentation of the different species was calibrated and contributions from other than the indicated species were subtracted, as well as background level, before normalising the signal intensity. In non-steady-state experiments, normalisation was performed by setting as 1 the concentration value observed before the switch. For SSITKA experiments, ^{12}CO and ^{13}CO concentrations were normalised by dividing their corrected MS signal intensities by the sum of both. Normalisation of $^{12}CO_2$ and $^{13}CO_2$ as well as $^{12}CH_4$ and $^{13}CH_4$ concentrations was performed in a similar manner.

TABLE 1

Changes in Gas Composition Introduced in Non-steady-state Transients

Experiment	From $CH_4 : CO_2 : (He + Ar)$	To $CH_4 : CO_2 : (He)$
Transient I	0 : 0 : 100	15 : 0 : 85
Transient II	15 : 15 : 70	0 : 0 : 100
Transient III	15 : 15 : 70	0 : 15 : 85
Transient IV	15 : 15 : 70	15 : 0 : 85

2.4. Temporal Analysis of Products

Transient pulse experiments were carried out in a TAP-2 reactor described in (10). Alternative (pump-probe) pulses of $^{12}CH_4$ and $^{13}CO_2$ were injected into the reactor via two high-speed valves (10–100 nmol per pulse). The catalyst sample (60 mg) was placed between two layers of 0.2–0.3 mm quartz particles. Prior to the experiments, catalysts were reduced for 1 h in a flow of pure hydrogen at 673 K, outgassed in vacuum, and heated to the reaction temperature (823 K).

2.5. In Situ DRIFT Spectroscopy

In order to determine the nature of accumulated adspecies under reaction conditions, *in situ* diffuse reflectance infrared Fourier transform (DRIFT) spectroscopy experiments were carried out in a Spectratech high temperature cell adapted to a Nicolet 550 spectrometer (18). All experimental conditions (catalyst loading and treatment, gas feeding, pressure, and temperature) applied for the above described transient kinetic experiments were exactly reproduced in the DRIFT cell.

3. RESULTS

3.1. Catalytic Testing

The catalytic activity of the Ru catalysts in the methane dry reforming reaction was tested at 823 K for 24 h. Table 2 reports the CH_4 and CO_2 reaction rates and H_2 selectivity after 30 min of reaction. The corresponding conversion levels of CH_4 are 14, 8, and 21%, and those of CO_2, 18, 13, and 30% for Ru/Al_2O_3, Ru/SiO_2, and Ru/HSAG, respectively, showing that for all three catalysts, CO_2 reaction rate is higher than that of CH_4. On the other hand, selectivity to H_2 diminishes as the ratio between CO_2 and CH_4 reaction rates increases. This indicates, as commonly reported for the dry reforming reaction, that the excess of CO_2, with

TABLE 2

Characterisation Data and Catalytic Properties for Methane Dry Reforming Reaction at 823 K over Ru-based Catalysts

Catalyst	Ru/Al_2O_3	Ru/SiO_2	Ru/HSAG
Ru loading (wt%)	0.64	0.72	1.00
Initial Ru dispersion (%)	51	13	35
CH_4 conversion rate[a] (μmol g^{-1} s^{-1})	35	21	26
CO_2 conversion rate[a] (μmol g^{-1} s^{-1})	46	33	36
H_2 selectivity[b] (%)	77	69	70
Deactivation rate[c] (μmol g^{-1} s^{-1} h^{-1})	0.59	0.90	0.21

[a] Methane and carbon dioxide reaction rates at 30 min.
[b] Moles of H_2 produced per 1/2 moles of CH_4 reacted at 30 min.
[c] Mean decrease in methane conversion rate per h during 24 h.

respect to the 1:1 stoichiometry of the reaction, is consumed via the reverse water gas shift (RWGS) reaction.

Figure 1 shows the change of the methane reaction rate per gram of catalyst with time on stream. Note in Table 2 that the initial specific Ru surface is approximately the same for Ru/Al_2O_3 and Ru/HSAG (1.45 and 1.55 m^2_{Ru}/g_{cat}, respectively) and 3.5 times smaller for Ru/SiO_2 (0.42 m^2_{Ru}/g_{cat}). However, these systems suffer sintering of the metal particles (19) when the temperature is raised from 673 (reduction temperature of fresh sample before H_2 chemisorption) to 823 K (reaction temperature). As can be seen in Fig. 1, the graphite-supported catalyst exhibits a rather stable activity, in contrast with the oxide-supported samples. The fastest deactivation rate is observed for Ru/SiO_2 (Table 2), which activity decays dramatically during the first 5 h. The apparent oscillatory behaviour observed in Fig. 1 was found irreproducible and therefore not related to a significant kinetic process (a slight instability of the furnace temperature could originate that behaviour).

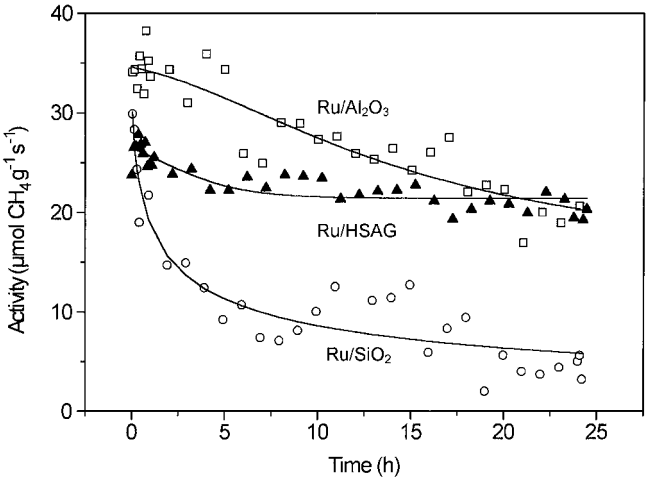

FIG. 1. CH_4 reaction rate in dry reforming at 823 K over Ru/Al_2O_3 (squares), Ru/SiO_2 (circles), and Ru/HSAG (triangles). Reaction mixture: 10% CH_4 + 10% CO_2 + 80% He. Total flow rate: 100 ml/min. 25 mg catalyst (50 mg for Ru/HSAG).

3.2. Non-Steady-State Transient Kinetic Experiments

3.2.1. Transient I: $He + Ar \rightarrow He + CH_4$. After switching from He to CH_4/He flow at 823 K at the reactor inlet, a low production of H_2 and CO is observed for Ru/Al_2O_3, while no products are detected for the other two catalysts. This residual production of H_2 and CO under diluted methane flow has already been reported for alumina-supported ruthenium (20). In the present case, the rates of H_2 and CO production 5 min after the switch are estimated as 6 and 2 μmol g^{-1} s^{-1}, respectively. These rates are approximately one order of magnitude smaller than those observed under dry reforming conditions (Table 2).

3.2.2. Transient II: $CH_4 + CO_2 + He + Ar \rightarrow He$ (Figs. 2a–2c). While for Ru/SiO_2 and Ru/HSAG catalysts, the CO_2 decay follows closely that of the inert tracer Ar, a slight delay is observed for Ru/Al_2O_3 between the two transient curves. This indicates that for the latter there is a certain accumulation of reversible CO_2 on the surface or creation of new sites for adsorption during the transient draining of this system. On Ru/Al_2O_3 and Ru/SiO_2, CH_4 and H_2 disappear even more rapidly than the inert tracer (Figs. 2a, 2b). This indicates that during this transient period, sites for irreversible methane and hydrogen adsorption are made available. The cracking of methane on new metallic sites and the reduction of surface oxygen by hydrogen into water (strongly tailing in all cases) could account for that observation. On Ru/HSAG, however, methane and hydrogen are slightly and markedly delayed with respect to Ar, respectively. Such delays could be due either (i) to some steam gasification of the graphite support into methane and hydrogen in the presence of water, or (ii) to the accumulation of CH_x species on the support and subsequent decomposition of these species leading mostly to the release of gaseous hydrogen and the formation of carbonaceous deposits on the graphite. The steam gasification is however unlikely since (i) CO should also be released together with hydrogen and (ii) the HSAG graphite is found to be very stable under the reactions conditions (stable surface area and stable catalytic activity).

3.2.3. Transient III: $CH_4 + CO_2 + He + Ar \rightarrow CO_2 + He$ (Figs. 2d–2f). When only methane is removed from the reaction mixture at 823 K, a faster decay of H_2 and a larger delay of CO and H_2O decay with respect to Transient II are observed for the three catalysts. This result brings again evidence of the oxidation of H_2 by CO_2 into H_2O and CO (RWGS).

3.2.4. Transient IV: $CH_4 + CO_2 + He + Ar \rightarrow CH_4 + He$ (Figs. 2g–2i). After the removal of CO_2 from the reaction mixture, a sudden increase in H_2 concentration is observed

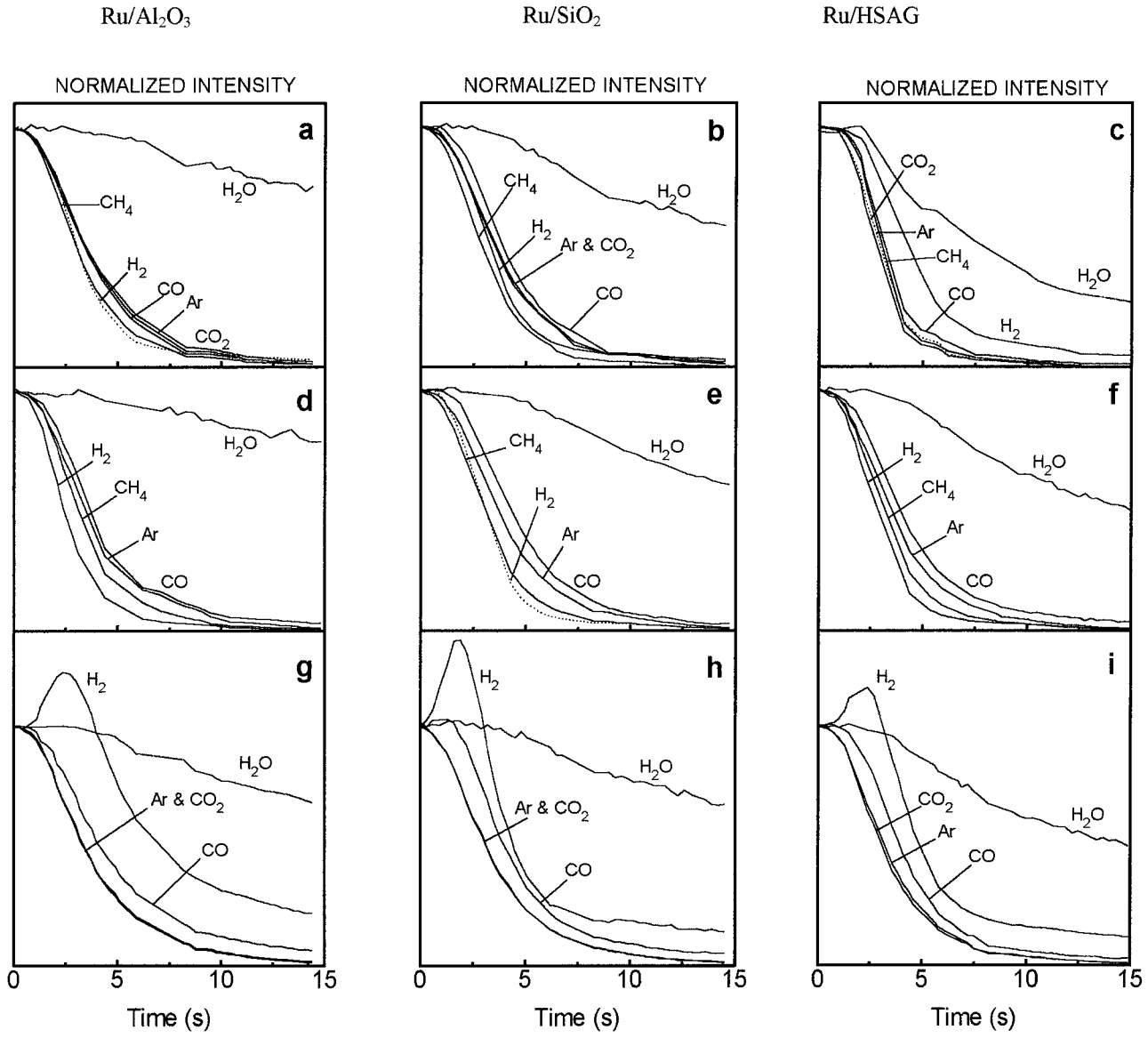

FIG. 2. Non-steady-state transient experiments at 823 K over Ru/Al_2O_3 (a, d, g), Ru/SiO_2 (b, e, h), and Ru/HSAG (c, f, i). Transient II, $CH_4 + CO_2 + He + Ar \rightarrow He$ (a, b, c); Transient III, $CH_4 + CO_2 + He + Ar \rightarrow CO_2 + He$ (d, e, f); and Transient IV, $CH_4 + CO_2 + He + Ar \rightarrow CH_4 + He$ (g, h, i).

in all cases. In agreement with the above interpretation, this increase must be attributed to the displacement of the RWGS towards WGS once CO_2 is removed favouring the H_2 production from methane cracking, at least until the metallic surface is saturated with carbon which inhibits progressively the cracking reaction. After reaching a maximum, the H_2 concentration decays quickly for Ru/SiO_2 and Ru/HSAG. On Ru/Al_2O_3, a slower decay of H_2 is observed, which points to a residual production of H_2 under CH_4 flow for several minutes, as already seen in Transient I.

3.3. Steady-State Isotopic Transient Kinetic Analysis

For the three catalysts, when $^{12}CH_4$ is replaced by $^{13}CH_4$ (time = 0 s) and stabilisation is reached, no $^{12}CH_4$ is detected among the products (Fig. 3). This result demonstrates that the dissociative activation of methane, evidenced in non-steady-state transient results, is not reversible. For the case of the Ru/HSAG sample, this result also tends to discard the hypothesis of a significant gasification of the graphite, which was proposed under transient conditions. It would therefore favour the alternative proposal of accumulation of CH_x entities on the graphite surface (see Transient II results).

Figure 3 reveals two types of behaviour concerning the carbon oxides produced under the $^{13}CH_4 + {}^{12}CO_2$ mixture. On the one hand, Ru/SiO_2 and Ru/HSAG plots show close stationary levels of ^{13}CO and $^{13}CO_2$ (and, therefore, ^{12}CO and $^{12}CO_2$). On the other hand, for Ru/Al_2O_3 these

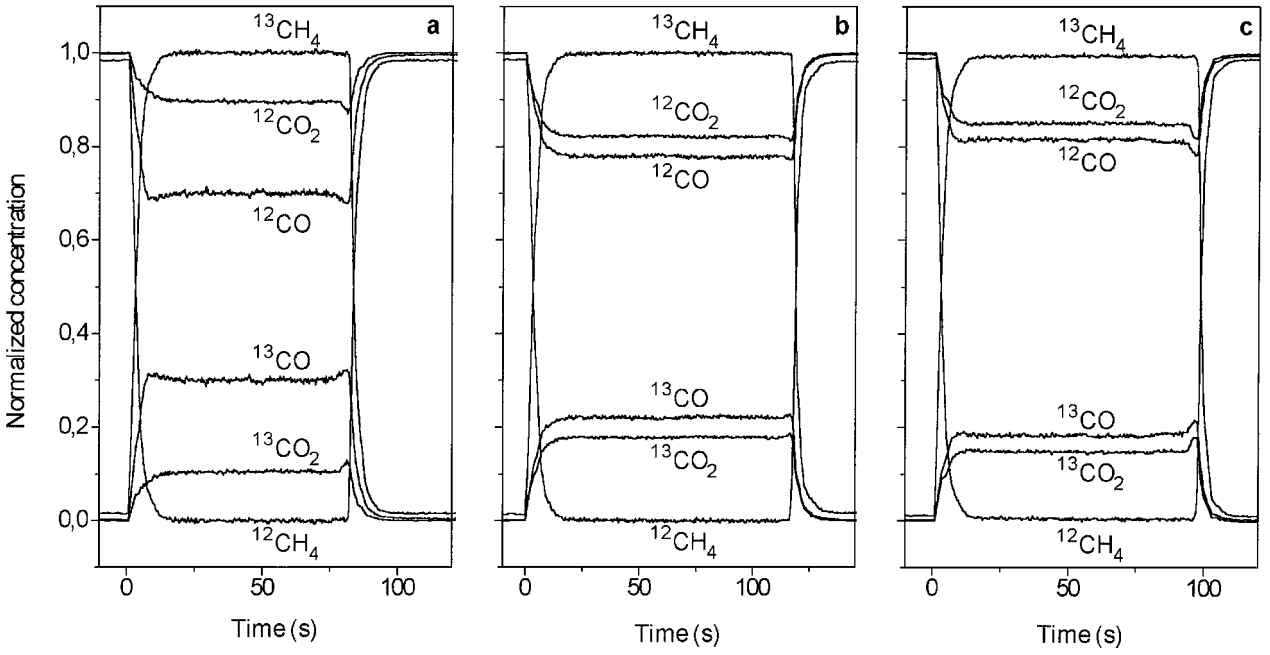

FIG. 3. SSITKA experiment at 823 K, switching from ($^{12}CH_4 + {}^{12}CO_2 + He$) to ($^{13}CH_4 + {}^{12}CO_2 + He + Ar$) and reverse. (a) Ru/Al_2O_3, (b) Ru/SiO_2, (c) Ru/HSAG.

stationary concentrations differ significantly, with a much higher concentration of ^{13}C in CO than in CO_2.

Figure 4 presents the normalised decay profiles of $^{13}CH_4$, ^{13}CO, and $^{13}CO_2$ resulting from the substitution of $^{13}CH_4$ by $^{12}CH_4$ in the reaction mixture. A slight delay of the $^{13}CO_2$ decay with respect to ^{13}CO on Ru/Al_2O_3 can be noticed (Fig. 4a). On the contrary, no delay is observed for Ru/SiO_2 and Ru/HSAG (Figs. 4b, 4c). This result suggests that, in accordance with the results obtained in Transient II (Figs. 2a–2c), CO_2 interacts with the alumina surface, but not with silica nor graphite.

For all catalysts, the CO decay curve is delayed with respect to methane (Fig. 4), which reveals the accumulation of intermediate species in the conversion of CH_4 into CO. If

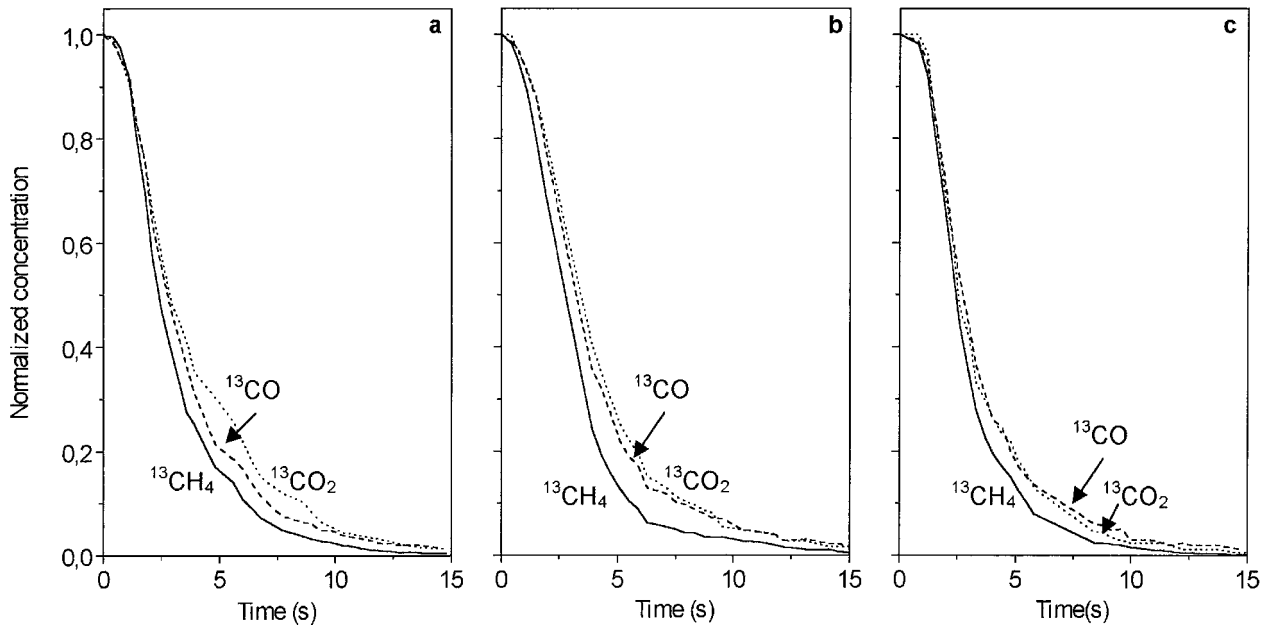

FIG. 4. Normalised decay responses of the labelled products when switching from ($^{13}CH_4 + {}^{12}CO_2 + Ar + He$) to ($^{12}CH_4 + {}^{12}CO_2 + He$) at 823 K (a) Ru/Al_2O_3, (b) Ru/SiO_2, (c) Ru/HSAG. Solid lines, $^{13}CH_4$; dashed lines, ^{13}CO; dotted lines, $^{13}CO_2$.

TABLE 3

Reactive Carbon Intermediates Accumulated on Ru Catalysts in the Dry Reforming Reaction at 823 K

Catalyst	τ (s)[a]	r_{CH_4} (μmol g^{-1} s^{-1})[b]	N (mg C g^{-1}cat)[c]	C/Ru$_s$[d]
Ru/Al_2O_3	0.50	34	0.20	0.5
Ru/SiO_2	0.89	28	0.30	2.7
Ru/HSAG	0.54	26	0.17	0.4

[a] Surface carbon intermediates residence time.
[b] CH_4 conversion rate.
[c] Carbon surface intermediates abundancy.
[d] Carbon to surface Ru atomic ratio.

one assumes that at least one irreversible elementary step exists in this route and that the rate limiting step leading to the formation of CO is pseudo first order, the steady-state rate of methane conversion r_{CH_4} into CO can be expressed as

$$r_{CH_4} = 1/\tau * N,$$

where τ is the mean residence time of the reacting intermediates (therefore $1/\tau$ the rate constant) and N is their concentration. Knowing r_{CH_4} (determined before or after the transient period) and τ (directly evaluated from the area between the CO and CH_4 normalized transient curves, expressed in time units), N values are straightforwardly obtained (17, 18). Table 3 reports these data, active carbonaceous intermediates being referred to as C at this stage of the study. Larger amounts of intermediate species are determined on Ru/SiO_2 with respect to the other catalysts. This difference is still more remarkable when referred to the metal surface (C/Ru$_s$ in Table 3); while for Ru/Al_2O_3 and Ru/HSAG the pool of active intermediates contains approximately one C per two surface Ru atoms, this ratio increases up to nearly three C per Ru$_s$ on Ru/SiO_2.

3.4. In Situ DRIFT Spectroscopy Experiments

Figure 5 shows parts of the infrared spectrum of the Ru/Al_2O_3 catalyst under a He flow at 823 K (Fig. 5a) and under the dry reforming mixture at the same temperature (Fig. 5b). The difference between the two spectra is reported in Fig. 5c for the 1300–1500 cm^{-1} range. The gas phase contribution, not shown in Fig. 5 for clarity, is observed at 3016 cm^{-1} (stretching) and between 1300 and 1350 cm^{-1} (deformation) for methane, at 2330 and 2340 cm^{-1} for CO_2, and at 2180 and 2100 cm^{-1} for CO. Bands at 1390–1440 (small and not well resolved), 1510 (strong), 1580 (strong), and 1610–1620 (shoulder) cm^{-1} develop under reaction conditions (Fig. 5c), completed with bands around 1000 cm^{-1} (not presented due to superimposed DRIFT noise, also accounting for the large band around 1350 cm^{-1}). They are characteristic of mono- and bidentate carbonates (other oxygenated adspecies such as carboxylate, bicarbonate, and formate could also be considered in this wavenumber range) (21, 22). All the latter bands disappear within a few minutes when CO_2 is removed from the gas inlet, showing that CO_2 interacts reversibly with the alumina surface as already deduced from SSITKA experiments. It can be pointed out that the time scale for CO_2 desorption in DRIFT transient experiments is much larger (few minutes) than the time scale for the previous kinetic transient experiments (few seconds). This relatively slow CO_2 desorption from alumina explains why no significant CO_2 desorption was observed on the alumina-supported catalyst during the Transients II and IV (Figs. 2a, 2g). At higher wavenumbers, no bands that could be assigned to adsorbed CO (2000–1800 cm^{-1}) are detected under reaction conditions.

In the region of OH stretching frequencies, bands at 3765 (shoulder), 3715, 3685, and 3670 and around 3600 (shoulder) cm^{-1} are observed on the fresh Ru/Al_2O_3 catalyst, which can be assigned to hydroxyl groups on the alumina surface (23). Under reaction conditions, an overall increase in intensity is observed in this region of the infrared spectrum, indicating the adsorption by the alumina support of water molecules produced by the reaction. No clear evidence of other changes in OH bands exists due to the superimposed overtones of the CO_2 present in the gas phase, in the region 3550–3700 cm^{-1}. When switching from the reaction mixture to Ar or a 10 vol.% CH_4 in Ar flow after 30 min of reaction, the integrated intensity of the spectrum in the region 3200–3800 cm^{-1} decreases due to the alumina dehydration (Fig. 6, solid symbols). However, under CH_4 flow a more intense decrease in the overall intensity takes place with respect to the same experience performed under Ar flow (square vs circle symbols, respectively).

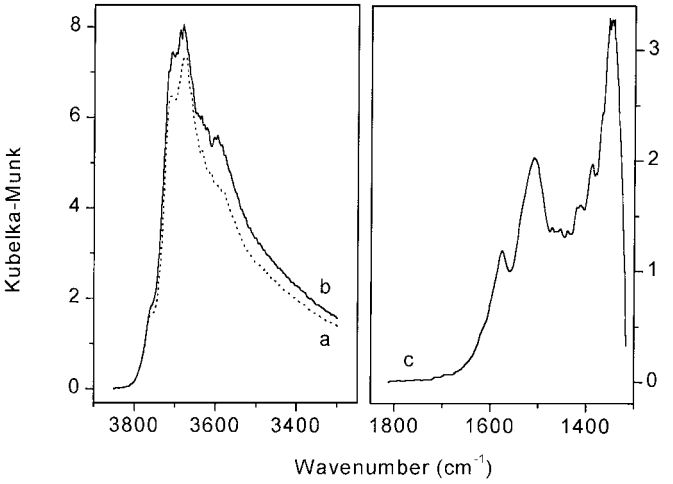

FIG. 5. DRIFT spectra of the Ru/Al_2O_3 catalyst at 823 K under (a) He flow and (b) after 10 min under the $CH_4 + CO_2$ reaction mixture. Spectrum (c) was obtained by subtracting (a) from (b). Spectra have been smoothed.

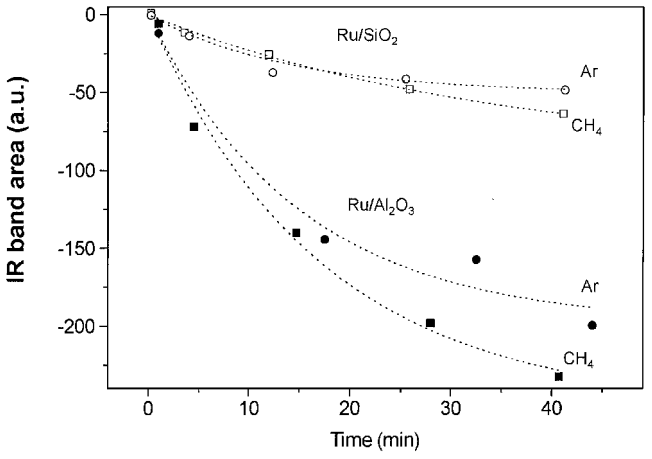

FIG. 6. Change in the integrated signal intensity of DRIFT spectra of Ru/Al_2O_3 (solid symbols), in the region 3200–3800 cm^{-1}, and Ru/SiO_2 (open symbols), in the region 3500–3800 cm^{-1}, when flowing Ar (circles) or 10 vol% CH_4 on Ar (squares) at 823 K after 30 min under the $CH_4 + CO_2$ reaction mixture at 823 K.

For Ru/SiO_2, no C–O vibrations are observed under reaction conditions and the hydroxyl bands characteristic of Si–OH groups only slightly decrease when switching to Ar or to CH_4 + Ar flows (Fig. 6, open symbols).

No reliable DRIFT analysis was possible on Ru/HSAG due to the weakness of the diffused beam.

3.5. Temporal Analysis of Products

The averaged normalised response for a series of alternating $^{12}CH_4$/Ar (9/1) and $^{13}CO_2$ pulses on the three ruthenium catalysts at 823 K are plotted in Fig. 7. Similar data obtained on Ru/SiO_2 were already reported in (10) as preliminary results. For all catalysts, when the methane pulse is introduced, it is partially converted and desorption of hydrogen follows, showing that methane is dissociatively adsorbed on Ru. The amounts of H_2 produced account for ca. 70 and 100% of the methane converted on Ru/Al_2O_3 and Ru/SiO_2, respectively, but only 5% for Ru/HSAG. For the latter, a trapping effect of hydrogen by the support as CH_x adspecies could explain that feature, as already proposed. Moreover, no water production is detected for the Ru/HSAG catalyst. Traces of H_2O (not shown in Fig. 7 for clarity) are produced when pulsing either CH_4 or CO_2 on Ru/Al_2O_3 and Ru/SiO_2.

The H_2 peak shows a long tailing for Ru/Al_2O_3. Some tailing is also observed for Ru/HSAG while, for Ru/SiO_2, H_2, and CH_4 pulses are almost superimposed. Following the methane pulse, a significant amount of ^{12}CO is also slowly desorbed on Ru/Al_2O_3, together with traces of ^{13}CO.

Pulsing $^{13}CO_2$ after $^{12}CH_4$ produces ^{12}CO and ^{13}CO as the main products for all catalysts. Also, small amounts of $^{12}CO_2$, delayed with respect to the $^{13}CO_2$ pulse, are observed. On Ru/SiO_2 and Ru/HSAG, both labelled and unlabelled carbon monoxides are desorbed simultaneously. However, when both reactants are pulsed together, a certain delay in the ^{12}CO desorption is observed.

On Ru/Al_2O_3, the pulse of $^{13}CO_2$ leads to the removal of the hydrogen that is still evolving after the methane pulse. The two different CO responses points out that there are two distinct sources of oxygen for the CO production on Ru/Al_2O_3. Simultaneous pulsing of $^{12}CH_4$ and $^{13}CO_2$ does not modify the response profiles. Comparatively broader pulses of carbon dioxide are also observed for Ru/Al_2O_3, which again indicates some interaction of this compound with the support.

In order to check if the distinct behaviour of the Ru/Al_2O_3 catalyst may be sensitive to the solid pretreatment, additional pump–probe TAP experiments were performed (i) on the Ru/Al_2O_3 catalyst previously submitted to a long series of CH_4 pulses at 823 K (Fig. 8a) and (ii) after a series of water vapour pulses at 823 K (Fig. 8b). For the former case, it can be seen that H_2 is no longer tailing and that CO is no longer produced when pulsing CH_4. After the steam treatment the H_2 tailing and the slow CO production after the methane pulse appear again.

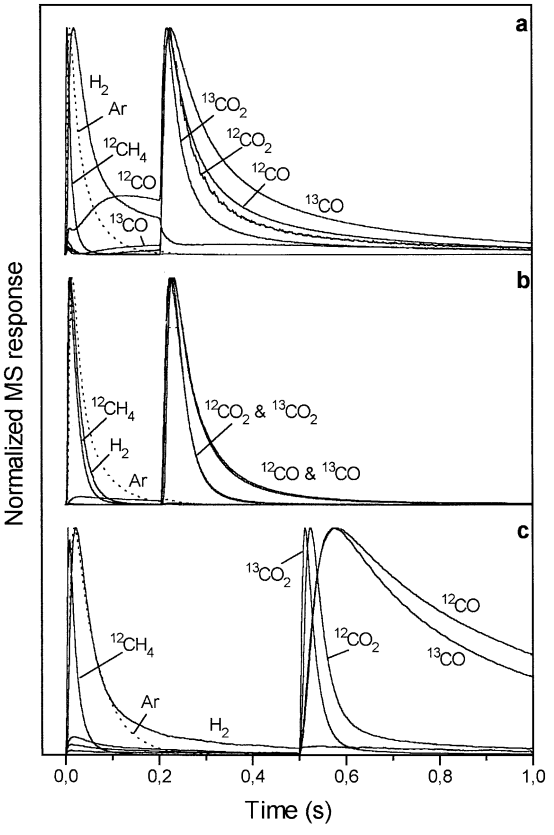

FIG. 7. TAP experiments with sequential $^{12}CH_4$/Ar (9/1) and $^{13}CO_2$/Ar pulses at 823 K on Ru/Al_2O_3 (a), Ru/SiO_2 (b), and Ru/HSAG (c).

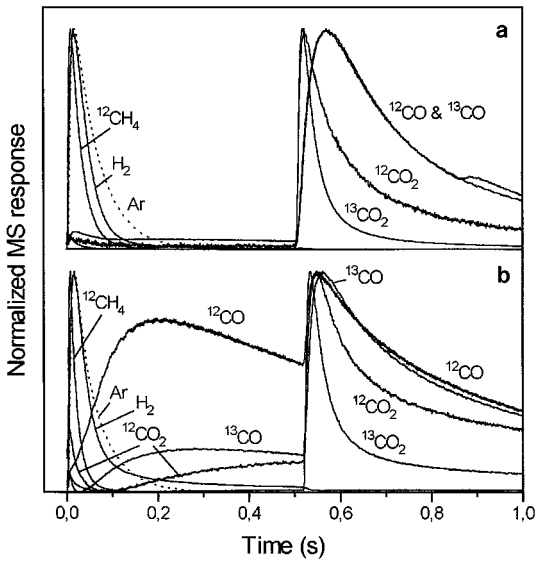

FIG. 8. TAP experiments with sequential $^{12}CH_4$/Ar (9/1) and $^{13}CO_2$/Ar pulses at 823 K on Ru/Al_2O_3 previously treated with a series of CH_4 pulses (a) and then with a series of H_2O pulses (b) at the same temperature.

4. DISCUSSION

Most of the results above reported show a marked influence of the support on the catalytic behaviour of Ru in the dry reforming of methane. Key mechanistic features are found however support independent, i.e., depending only on the nature of the metal. Let us first discuss the two processes that appear support dependent: catalyst stability and side reactions.

Catalyst stability. The differences in catalyst ageing—$HSAG < Al_2O_3 \ll SiO_2$ (Fig. 1)—cannot be ascribed to some particle size effect (as it was found for Ni catalysts (24)) since the initial dispersion of Ru ranks as $Al_2O_3 > HSAG > SiO_2$ (Table 2) and after sintering at 823 K the values of Ru dispersion are below 10% (19). This absence of correlation between ageing and Ru dispersion is in line with the general statement that the CO_2 reforming at high temperature is structure insensitive (8). The carbon deposition and poisoning remain therefore the main origin of the ageing process. Indeed, it is well known that carbon which may come both from methane and carbon dioxide is first produced as an active intermediate (under a monomeric form, more or less hydrogenated) which may further either be oxidized into CO or step-wise transform into polymeric, encapsulating, and/or filamenteous graphite (6, 8, 24). The detailed process of deactivation will not be discussed here, which would require a specific study, but only the possible role of the support in the initial key steps of carbonaceous adspecies formation. As a matter of fact, the lifetime and accumulation of these coke precursors may directly determine the catalyst ageing.

Side reactions. Catalytic tests and transient kinetic results have proven that, together with the main (dry reforming) reaction, RWGS takes place under the studied reaction conditions. However, the extension of the RWGS reaction (by comparison with the thermodynamic equilibrium) seems to be also influenced by the nature of the support. The yield of the RWGS reaction, which can be correlated with the decrease of H_2 selectivity, is similar for Ru/SiO_2 and Ru/HSAG but lower for Ru/Al_2O_3.

Another side reaction to consider is the reactivity of the support itself. While the silica support seems to be inert, alumina and graphite demonstrate a certain reactivity, as shown by DRIFT for alumina (carbonate, carboxylate formation/decomposition depending on the CO_2 partial pressure) or by observing hydrogen and methane release during transient experiments for graphite.

The analysis of the kinetic data may inform us about the specific roles played by the metal phase and eventually by the different supports.

Role of the Ruthenium Phase

Methane activation. TAP results (Fig. 7) show that H_2 is formed on the CH_4 pulse whatever be the support, demonstrating that methane is activated on Ru. This activation is found in addition to be irreversible since no $^{12}CH_4$ is detected in SSITKA experiments when switching from $^{12}CH_4$ to $^{13}CH_4$ (Fig. 3). This irreversible cracking could be considered as a specific property of the noble metals, since over Pt, a similar step is proposed (14) while on a non-noble metal like Ni, a largely reversible activation was observed under the same conditions (10, 11, 18).

The fast decay of CH_4 and H_2 concentration in Transient II (from reaction mixture to helium) for Ru/SiO_2 and Ru/Al_2O_3 (Fig. 2) also supports an irreversible activation step. The marked delay of the H_2 transient curve for Ru/HSAG could be related to the accumulation of CH_x species which decompose under He stream ($CH_x \rightarrow C + (x/2)H_2$) as already mentioned and discussed later.

For at least one catalyst, namely Ru/SiO_2 (for which no support effect is expected) the selectivity of methane cracking to hydrogen is 100% upon the TAP methane pulse. The methane cracking step can therefore be written as

$$CH_4 + x\ Ru \rightarrow Ru_{x-4}\text{-}C + 4\ Ru\text{-}H \qquad [1]$$

$$2\ Ru\text{-}H \rightleftarrows 2\ Ru + H_2 \qquad [2]$$

Indeed, step [1] represents a global reaction that does not exclude fast and step-wise intermediate dehydrogenation steps. The structure of the dehydrogenated surface carbon Ru_{x-4}-C deserves further comments.

From SSITKA, a steady-state accumulation of one active C for two Ru surface atoms is found for the most stable catalysts (Ru/Al_2O_3 and Ru/HSAG in Table 3). Although no

stable structure of Ru carbide is known from the literature, this could indicate that the most likely stoichiometry for the surface carbon is Ru_2C, at least for the two above quoted catalysts. Such a stoichiometry would again be specific of this noble metal since a value closer to one active C for three metal surface atoms was found for the case of nickel-based catalysts (17). For the case of a less stable catalyst like Ru/SiO_2, the much larger SSITKA ratio $C/Ru_S = 2.7$ would indicate that the primarily formed active carbon Ru_2C could rapidly (and reversibly) transform into a more polymerised form (still active on the surface). Due to the rather low reaction temperature (823 K), such a surface carbon polymer could be of a similar nature as the chain precursors observed under Fischer–Tropsch conditions. However, no C_n species may be formed for the present case since instead of being step-wise hydrogenated, the activated carbon adspecies suffer an oxidative attack leading to carbon monoxide. This brings us to analyse the process of carbon dioxide activation, as oxygen supplier for carbon oxidation.

Carbon dioxide activation. The occurrence of the RWGS reaction, whatever the type of support, brings evidence that CO_2 is activated on Ru. In addition, under a $^{13}CH_4 + {}^{12}CO_2$ reaction mixture, the four labelled and unlabelled CO and CO_2 species are produced (Fig. 3), which demonstrates that the dissociation of CO_2 takes place reversibly. Thus, the possible steps of carbon dioxide activation can be written as

$$CO_2 + Ru \rightleftarrows Ru\text{-}CO_2 \quad [3]$$

$$Ru\text{-}CO_2 + Ru \rightleftarrows Ru\text{-}CO + Ru\text{-}O \quad [4]$$

$$Ru\text{-}CO + Ru \rightleftarrows Ru\text{-}C + Ru\text{-}O \quad [5]$$

$$Ru\text{-}CO \rightleftarrows CO + Ru \quad [6]$$

The fast decay of CO_2 in Transients II and IV over Ru/SiO_2 and Ru/HSAG (Fig. 2) indicates that under reforming conditions there is no accumulation of CO_2 that may rapidly desorb. This means that step [4] is faster than step [3], both steps forming probably only one merged kinetically significant step:

$$CO_2 + 2Ru \rightleftarrows Ru\text{-}CO + Ru\text{-}O \quad [4']$$

On Ru/SiO_2 and Ru/HSAG, all these steps must be in fast equilibrium as the mixture of carbon oxides in SSITKA almost reaches the isotopic scrambling equilibrium (the equilibrium would correspond to identical normalized concentrations of ^{12}CO and $^{12}CO_2$ and, therefore, ^{13}CO and $^{13}CO_2$, in Fig. 3). In contrast, for Ru/Al_2O_3, concentration levels far from those of the isotopic scrambling equilibrium are obtained. This effect, which cannot be ascribed to any effect of strong CO_2 adsorption by alumina since it would lead to O and not to C scrambling, agrees with the lower extent of the RWGS reaction with respect to Ru/SiO_2 and Ru/HSAG. Another type of support effect has to be considered to account for such behaviour, as discussed later.

In TAP experiments, when pulsing $^{13}CO_2$ after $^{12}CH_4$ on ruthenium, ^{12}CO and ^{13}CO are desorbed simultaneously (Fig. 7). This means that though from the above scheme CO is formed both from CO_2 dissociation (step [4′]) and from surface carbon oxidation (reverse step [5]), the desorption of CO (step [6]) is the slowest step among the equilibria [3] to [6]. However, this step must be fast enough at this temperature so that no large amounts of adsorbed CO accumulate, which would have been detected by *in situ* DRIFT spectroscopy. Note that on Ni catalysts, a marked difference in the two ^{12}CO and ^{13}CO TAP responses allowed us to conclude that the reverse step [5] of carbon oxidation was limiting the reforming process (10, 11).

For Ru/SiO_2 and Ru/HSAG, no delay is observed between CO_2 and CO decays in SSITKA experiments (Figs. 4b, 4c). This indicates that the oxygen coverage of ruthenium is small, which again supports the conclusion that the steps [3] to [5] are fast. On Ru/Al_2O_3 (Fig. 4a) the CO_2 decay with respect to CO has to be ascribed to a support effect, as discussed later.

H_2O production. In order to account for the side production of water, the following steps should be included in the mechanism for Ru particles supported on inert materials (SiO_2, HSAG):

$$Ru\text{-}O + Ru\text{-}H \rightleftarrows Ru\text{-}OH + Ru \quad [7]$$

$$2\ Ru\text{-}OH \rightleftarrows Ru\text{-}O + Ru + H_2O \quad [8]$$

The combination of these steps with the previous ones leads to the overall RWGS equilibrium. It points out that the H_2 selectivity of the reforming reaction (Table 2) depends directly on the stability (or reactivity) of the Ru–O adspecies which reacts competitively either with surface carbon (step [5]) to form CO or with surface hydrogen (step [7]) to form water. Again, the fast equilibria [7] and [8] are not expected to lead to large accumulation of intermediates such as Ru–OH hydroxyls that would have been detected by *in situ* DRIFT (in addition to the well-detected OH groups of the supports).

Role of the Support

Alumina. In contrast with the other supports, γ-alumina presents under the reforming conditions a large concentration of hydroxyl groups ranging from basic to acid character, as detected by *in situ* DRIFT (3765, 3715, 3685, 3670 cm^{-1}). A residual production of H_2 and CO is observed on Ru/Al_2O_3 when the reacting feed is switched to diluted methane at 823 K (Transient IV). In addition, a larger consumption of alumina OH groups is observed during the same Transient IV by comparison with the consumption due to the support dehydration under inert flow (Fig. 6). Also, a long H_2 tailing and a slow ^{12}CO desorption takes

place when the pulse of $^{12}CH_4$ is introduced in TAP experiments (Fig. 7a). All these results indicate that in addition to the processes specifically related to the ruthenium phase, a continuous feeding of the ruthenium surface by OH groups from the alumina interface takes place as follows:

$$\text{Al-OH} + \text{Ru} \rightarrow \text{RuOH} + \text{Al}\,\square \qquad [9]$$

These OH groups provide through equilibrium [7] a continuous second source of (i) H atoms that desorb as H_2 following step 2 and (ii) O atoms that react with the carbon atoms generated by CH_4 dissociation that produces CO, following the reverse step [5] and step [6].

Within this scheme the TAP experiments (Fig. 7a) can now be described as follows: (i) the continuous flux of ^{12}CO observed after the $^{12}CH_4$ pulse arises from the oxidation of ^{12}C deposited after methane cracking and is combined with the flux of ^{13}CO after the pulse of $^{13}CO_2$, the latter arising from the $^{13}CO_2$ dissociation. Some ^{13}C also formed from ^{13}CO dissociation (step [5]) will react with O from OH groups to give the slight flux of ^{13}CO also observed after the methane pulse. (ii) The tailing pulse of H_2 observed after the methane pulse combines the main flux coming directly from methane cracking (narrow part of the pulse) and the hydrogen continuously fed by the OH groups of alumina (tailing part). This tailing production of hydrogen is abruptly decreased during the CO_2 pulse due to the large production of surface oxygen from the CO_2 decomposition which temporarily hinders the OH dissociation over Ru (displacement of equilibrium [7]).

This reverse spillover of OH groups is confirmed by results in Fig. 8 showing that H_2 is no longer tailing and that CO is not produced upon the CH_4 pulse when OH groups have been removed from alumina by a long series of CH_4 pulses. Inversely after a series of water vapour pulses at 823 K which enhances the feeding of the Ru surface with alumina OH groups, the H_2 tailing as well as the continuous CO production are markedly increased (Fig. 8b).

The consumed alumina hydroxyl groups are regenerated by the water formed during the process through the RWGS reaction. Thus, this extra source of Ru–OH adspecies explains the lower extent of the RWGS reaction observed on alumina with respect to SiO_2 and HSAG by a displacement towards the water production of the equilibrium [8]. Similarly the higher H_2 selectivity (Table 2) derives from the displacement towards Ru–H species (therefore H_2 production) of the equilibrium [7]. Such displacement also increases the surface concentration of Ru–O species. This in turn favours the CO formation at the expense of the carbon polymerisation and further graphitisation, in agreement with the relative stability of the catalyst (Fig. 1).

A close process of spillover between alumina and metal but via the migration of water molecules was recently proposed by Wang *et al*. for the partial oxidation of methane over Rh/Al_2O_3 (26).

A second major property of alumina is to directly and strongly interact with CO_2:

(i) a delay of CO_2 decay with respect to CO is observed in SSITKA (Fig. 4),

(ii) the formation of carbonate and/or carboxylate under reaction conditions is observed by *in situ* DRIFT (Fig. 5).

Such interaction with alumina can be written as follows for carbonate (bidentate) and carboxylate, respectively:

$$2\ \text{Al-OH} + \text{CO}_2 \rightleftarrows \text{Al-O-CO-O-Al} + \text{H}_2\text{O} \qquad [10]$$

$$4\ \text{Al-OH} + 2\ \text{CO}_2 \rightleftarrows 2\ \text{Al-O-CO-OH} + \text{Al-O-Al} + \text{H}_2\text{O} \qquad [11]$$

Other more complexe processes which would involve the reaction of carbonates with hydrogen to form formate species further on decomposed into CO (as proposed by Amenomiya (27) for explaining the WGS activity on alumina) cannot be excluded though no direct evidence of their occurrence is provided in the present study.

Graphite. The large delay of H_2 in Transient II experiments on Ru/HSAG (Fig. 2), the H_2 tailing that follows the methane pulse in TAP experiment (Fig. 7c), and the very low H_2 selectivity (5%) are well accounted for by the accumulation of hydrogen rich CH_x species over the graphite support and/or over the Ru phase. Thus, when the running catalyst is purged by He (Transient II), these accumulated species decompose into gaseous hydrogen. Under the TAP conditions (sample maintained under vacuum between the pulses), the dehydrogenated support would act as a hydrogen trap through CH_x entities (formed either directly from the reaction of gaseous hydrogen with surface carbon or from the migration of CH_x species from the Ru to the graphite surface). Under steady-state conditions, the migration of CH_x entities to the support and/or the availability of a second source of hydrogen at the interface of the Ru particles/support would hinder carbon graphitisation and encapsulation on the Ru particles. This would explain the prominent stability of this catalyst, as observed in Fig. 1.

Silica. No support effect is detected for the case of silica, as expected from a rather inert material with stable hydroxyl groups under steady-state or transient conditions, as shown in Fig. 6. This leads to a larger accumulation of surface carbon over the Ru phase (Table 2) and therefore to a marked trend to polymerisation and graphitisation, resulting in a fast deactivation as shown in Fig. 1.

5. CONCLUSIONS

The kinetic behaviour of the three different Ru catalysts is shown to be monitored essentially by the chemistry which develops over the ruthenium phase. Thus, a mechanistic scheme specific of this metal (and by extension of noble metals, at variance with non-noble metals like nickel) is

derived, indicating an irreversible methane activation and a relatively slow step of CO desorption. In addition to the metal chemistry, major support effects such as the continuous back spillover of alumina hydroxyl groups, the accumulation of CO_x species on the alumina surface and of CH_x species on the graphite are also found to contribute to the overall process, with direct effects on the catalyst stability.

ACKNOWLEDGMENTS

This work was supported by a joint programme CNRS-CSIC and by the CICYT of Spain (Project MAT96-0859-CO2-O2). PFA acknowledges a scholarship grant from the Comunidad de Madrid, Spain.

REFERENCES

1. Rostrup-Nielsen, J. R., *Catal. Today* **18**, 305 (1993).
2. Teuner, S., *Hydrocarb. Process.* **May**, 106 (1985).
3. Gadalla, A. M., and Bower, B., *Chem. Eng. Sci.* **43**, 3049 (1988).
4. Gadalla, A. M., and Sommer, M. E., *Chem. Eng. Sci.* **44**, 2825 (1989).
5. Richardson, J. T., and Paripatyadar, S. A., *Appl. Catal.* **61**, 293 (1990).
6. Rostrup-Nielsen, J. R., and Bak-Hansen, J. H., *J. Catal.* **144**, 38 (1993).
7. Perera, J. S. H. Q, Couves, J. W., Sankar, G., and Thomas, J. M., *Catal. Lett.* **11**, 219 (1991).
8. Mark, M. F., and Maier, W. F., *J. Catal.* **164**, 122 (1996).
9. Erdohelyi, A., Cserényi, J., and Solymosi, F., *J. Catal.* **141**, 287 (1993).
10. Schuurman, Y., Kroll, V. C. H., Ferreira-Aparicio, P., and Mirodatos, C., *Catal. Today* **38**, 129 (1997).
11. Schuurman, Y., Marquez-Alvarez, C., Kroll, V. C. H., and Mirodatos, C., *Catal. Today* **46**, 185 (1998).
12. Bitter, J. H., Seshan, K., and Lecher, J. A., *J. Catal.* **176**, 93 (1998).
13. Schuurman, Y., and Mirodatos, C., *Appl. Catal. A: Gen.* **151**, 305 (1997).
14. van Keulen, A. N. J., Seshan, K., Hoebink, J. H. B. J., and Ross, J. R. H., *J. Catal.* **166**, 306 (1997).
15. Buyevskaya, O. V., Wolf, D., and Baerns, M., *Catal. Lett.* **29**, 249, 261 (1994).
16. Mallens, E. P. J., Hoebink, J. H. B. J., and Marin, G. B., *J. Catal.* **160**, 222 (1996).
17. Mirodatos, C., *Catal. Today* **9**, 83 (1991).
18. Kroll, V. C. H., Swaan, H. M., Lacombe, S., and Mirodatos, C., *J. Catal.* **164**, 387 (1996).
19. Ferreira-Aparicio, P., Guerrero-Ruiz, A., and Rodriguez-Ramos, I., *Appl. Catal. A: Gen.* **170**, 177 (1998).
20. Ferreira-Aparicio, P., Rodriguez-Ramos, I., and Guerrero-Ruiz, A., *Appl. Catal. A: Gen.* **148**, 343 (1997).
21. Little, L. H., "Infrared Spectra of Adsorbed Species." Academic Press, New York, 1996.
22. Angell, C. L., and Howel, M. V., *J. Phys. Chem.* **74**, 2737 (1970); Nakamoto, K., "Infrared Spectra of Inorganic and Coordination Compounds." Wiley, London, 1963.
23. Knözinger, H., and Ratnasamy, P., *Catal. Rev. Sci. Eng.* **17**, 31 (1978).
24. Kroll, V. C. H., Swaan, H. M., and Mirodatos, C., *J. Catal.* **161**, 409 (1996).
25. Nakamura, J., Aikawa, K., Sato, K., and Uchijima, T., *Catal. Lett.* **25**, 265 (1994).
26. Wang, D., Dewaele, O., De Groote, A. M., and Froment, G. F., *J. Catal.* **159**, 418 (1996).
27. Amenomiya, Y., and Pleizer, G., *J. Catal.* **76**, 345 (1982).